Planetary and Space Science 119 (2015) 24–35

Contents lists available at ScienceDirect

Planetary and Space Science

journal homepage: www.elsevier.com/locate/pss

Surface charging and electrostatic dust acceleration at the nucleus of comet 67P during periods of low activity

T.A. Nordheim [a,b,*], G.H. Jones [a,b], J.S. Halekas [c], E. Roussos [d], A.J. Coates [a,b]

[a] Mullard Space Science Laboratory, University College London, Dorking, UK
[b] Centre for Planetary Sciences at UCL/Birkbeck, University College London, London, UK
[c] Department of Physics and Astronomy, University of Iowa, Iowa City, IA, USA
[d] Max Planck Institute for Solar System Research, Göttingen, Germany

ARTICLE INFO

Article history:
Received 28 January 2015
Received in revised form
17 June 2015
Accepted 17 August 2015
Available online 28 August 2015

Keywords:
Plasma interaction with unmagnetized bodies
Solar wind
Plasma
Surface charging
Comets
Dust

ABSTRACT

We have investigated through simulation the electrostatic charging of the nucleus of Comet 67P/Churyumov–Gerasimenko during periods of weak outgassing activity. Specifically, we have modeled the surface potential and electric field at the surface of the nucleus during the initial Rosetta rendezvous at 3.5 AU and the release of the Philae lander at 3 AU. We have also investigated the possibility of dust acceleration and ejection above the nucleus due to electrostatic forces. Finally, we discuss these modeling results in the context of possible observations by instruments on both the Rosetta orbiter and the Philae lander.

1. Introduction

Comets are constantly exposed to incoming solar wind plasma, which in the rest frame of the comet is supersonic. Due to solar insolation, cometary volatiles at the surface and within the subsurface may sublimate and be expelled from the nucleus. A large fraction of these ejected neutrals become ionized and are "picked up" by the solar wind motional electric field, transferring momentum and energy from the solar wind, causing it to decelerate near the nucleus (e.g. Coates, 1997, 2004). Eventually, as outgassing rates increase, the solar wind may be sufficiently decelerated ("mass loaded") for several plasma structures to form, including a weak bow shock (Biermann et al., 1967) and a diamagnetic cavity where the plasma is purely cometary in origin (Ip and Axford, 1987). However, as cometary gas production rates typically vary by several orders of magnitude depending on the comet–Sun distance, the interaction between the comet and the solar wind will change substantially depending on its activity phase (e.g. Cravens and Gombosi, 2004; Hansen et al., 2007; Rubin et al., 2014). In the case of a comet that is weakly outgassing, either intrinsically so, or when a productive comet is far from the Sun, the resulting mass loading rate will be insufficient to form these plasma boundaries, and the un-shocked solar wind will be able to flow directly onto the nucleus.

Comet 67P/Churyumov–Gerasimenko is a relatively weakly outgassing comet, with a predicted outgassing rate at perihelion ($\sim$1.29 AU) of $\sim 10^{27}$ molecules/s (Snodgrass et al., 2013), in comparison to that of comet 1P/Halley during its most recent apparition ($\sim 10^{30}$ molecules/s) (Huddleston et al., 1990; Weaver et al., 1986). The Rosetta spacecraft rendezvoused with comet 67P in August 2014, when the comet–Sun distance was roughly 3.5 AU. During this initial stage of the encounter, the comet was expected to be only weakly outgassing, with a predicted gas production rate of $\sim 10^{25}$ molecules/s (Snodgrass et al., 2013). Koenders et al. (2013) investigated the predicted evolution of plasma structures around 67P during the Rosetta escort phase using MHD and hybrid models. Their work predicted that 67P's cometary bow shock is only fully established when the comet–Sun distance is less than 1.35 AU, and that the magnetic pile up region and diamagnetic cavity appear when the comet–Sun distance is less than 2 AU, which occurs in April 2015. Thus, early in the Rosetta escort phase and during the touchdown of the Philae lander, it is expected that the un-shocked solar wind may flow directly onto the cometary nucleus.

Objects exposed to inflowing plasma and solar UV photons experience charging currents due to electron and ion bombardment, photoemission, and secondary electron emission (Whipple, 1981).

* Corresponding author at: Mullard Space Science Laboratory, University College London, Dorking, UK. Tel.: +44 7504 305 104; fax: +44 1483 278312.
E-mail address: tom.nordheim.10@ucl.ac.uk (T.A. Nordheim).

http://dx.doi.org/10.1016/j.pss.2015.08.008

For typical solar system materials, the electrical conductivity is sufficiently low that different regions on the surface may charge to different electrostatic potentials, depending on the local solar insolation and plasma flow geometries, as illustrated in Fig. 1. Although predicted to occur on a number of planetary bodies, this effect has so far only been reported to be observed in-situ at the Earth's moon (e.g. Freeman and Ibrahim, 1975; Halekas et al., 2002) and at Saturn's moons Hyperion (Nordheim et al., 2014) and Rhea (Jones et al., 2011; Santolík et al., 2011). The effect is also well-established to occur on spacecraft themselves. It has been predicted that surface charging may also occur on cometary nuclei during periods of low outgassing activity, when solar wind plasma and solar UV photons are allowed direct access to the nucleus (Mendis et al., 1981). It has also been suggested that surface charging of the nucleus may lead to electrostatic levitation of small dust particles (Flammer et al., 1986; Juhász and Szegő, 1998; Mendis et al., 1981) and that electrostatic dust blow-off may explain sudden changes in the observed brightness of comet Halley at large heliocentric distances (Flammer et al., 1986). As suggested in the recent review given by Mendis and Horányi (2013), the nucleus of comet 67P may exhibit surface charging and dust levitation during the initial part of the Rosetta escort phase when the comet is expected to be only weakly outgassing. The present work considers surface charging of the 67P nucleus during periods of weak activity, such as was the case during the initial encounter and early escort phase of the Rosetta mission. Thus we aim to provide context for the interpretation of data from the Rosetta orbiter and Philae lander, the latter which landed on comet's nucleus on November 12th 2014, when the comet–Sun distance was ~3 AU.

2. Modeling approach

In this section we present our approach for modeling of surface charging of the 67P nucleus as well as emission of charged submicron dust grains from the surface. In Section 2.1 we give the modeling approach for calculating the surface potential on the dayside nucleus. In Section 2.2 we expand on this by presenting a treatment of the solar wind plasma wake, which allows us to calculate surface potentials on the nightside (downstream) nucleus. In Sections 2.3 and 2.4 we outline how charged dust grains may be electrostatically accelerated away from the nucleus and how the flux of electrostatically emitted charged nanodust may be calculated.

2.1. Surface charging of the dayside nucleus

In order to calculate the electrostatic potential on the surface of the 67P nucleus, we have made use of the formulation of Manka (1973) for the Earth's Moon in the solar wind as implemented by Roussos et al. (2010), which for a given Solar Zenith Angle (SZA) solves the current balance

$$I_{\text{ion}} + I_{\text{electron}} + I_{\text{photoelectron}} + I_{\text{secondary}} = 0$$

Due to the large thermal velocity of solar wind electrons compared to the solar wind flow velocity, at every point, they are nearly isotropically incident on the surface of the nucleus and the electron current is proportional to the local electron temperature and density. The gyroradius of the relatively cold solar wind protons will be much larger than the size of the 67P nucleus. However, since the solar wind velocity is much greater than the thermal velocity of the ions, the ion current depends on the flow angle as well as the ion temperature and density.

For the solar wind parameters during the initial Rosetta encounter and Philae landing, we have taken those of Stubbs et al. (2014) at 1 AU and scaled these according to the radial scaling relations provided in Table 1. The photoelectron current is taken from that of Sternovsky et al. (2008) at the subsolar point of the Earth's moon and scaled to the orbital distance of the comet. The current due to emission of secondary electrons depends on the

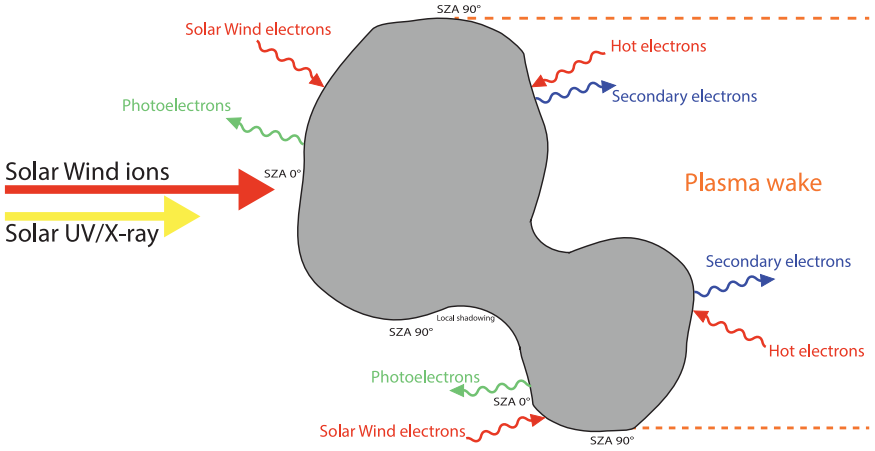

Fig. 1. Plasma interactions and surface charging of a weakly outgassing or inert cometary nucleus with a "double-lobe" structure.

Table 1
Model input parameters for Rosetta initial rendezvous (3.5 AU) and lander touchdown (3.0 AU).

Parameter	1 AU	3.0 AU	3.5 AU	Scaling	Note
T_e [eV]	12.1	4.45	3.87	$R^{-0.91}$	Scaling: Phillips et al. (1995)
T_i [eV]	8.6	3.99	3.58	$R^{-0.7}$	Scaling: Gazis and Lazarus (1982)
V_{flow} [km s^{-1}]	400	400	400		Negligible change – McComas et al. (2000)
Plasma density [cm^{-3}]	10	1.11	0.82	R^{-2}	Scaling: McComas et al. (2000)
E_{max} [eV]	420 eV	420	420		Tiersch and Notni (1989)
δ_{max}	2.5	2.5	2.5		Tiersch and Notni (1989)
I_p [A m^{-2}]	$5.05E^{-06}$	$5.61E^{-07}$	$4.12E^{-07}$	R^{-2}	Sternovsky et al. (2008)

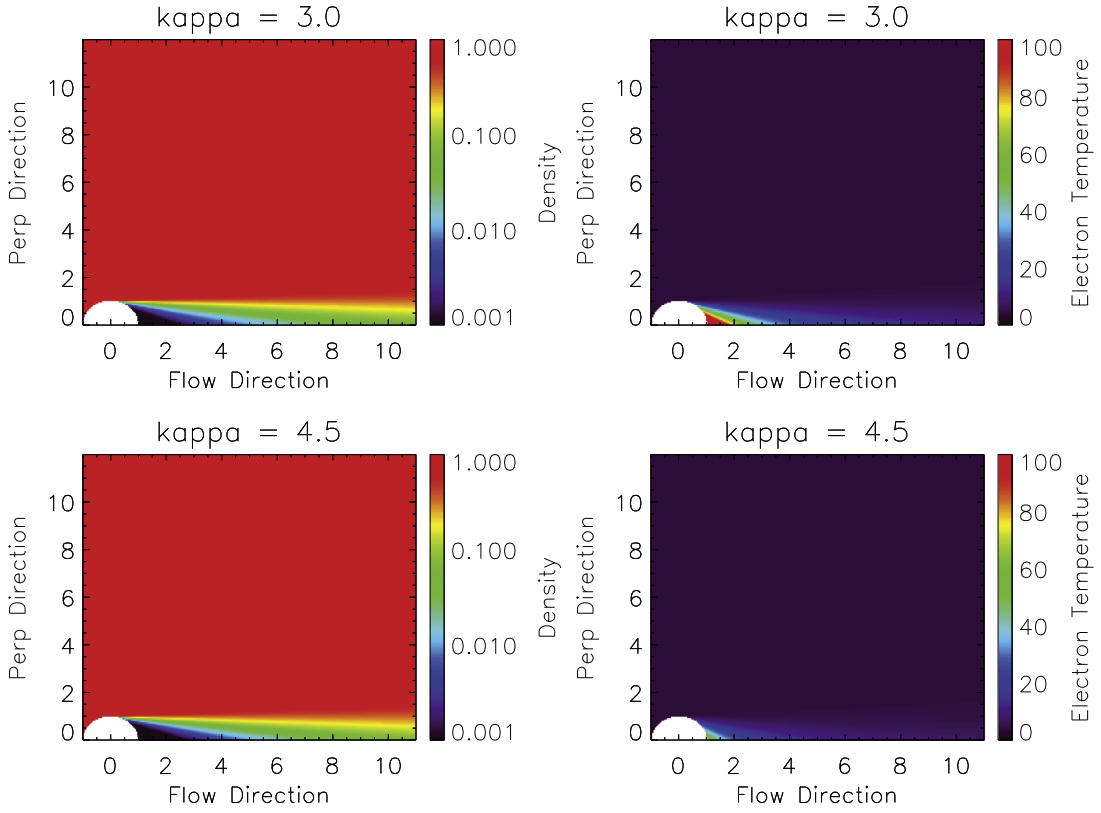

Fig. 2. Output of the self-similar model for the comet's plasma wake for solar wind electron distributions with κ values of 3 (top) and 4.5 (bottom). The left hand plot shows the plasma density and the right hand plot shows the electron temperature. Coordinates are in body radii (1 R_{nucleus}=2 km).

electron current and the secondary emission yield (δ), where δ is determined according to the angle-averaged form of the Katz formula (Jurac et al., 1995; Katz et al., 1977; Whipple, 1981)

$$\delta(E) = 5.08\delta_{\max}\frac{E}{E_{\max}}\frac{Q-1+\exp(-Q)}{Q^2}$$

where E is the average energy of the incident electrons, $\delta_{\max}$ is the maximum secondary emission yield, $E_{\max}$ is the energy at which the maximum secondary emission yield occurs and $Q = 2.28(E/E_{\max})^{1.35}$. Assuming that the nucleus is covered by a global dust mantle (Brin and Mendis, 1979; Heggy et al., 2012; Prialnik and Bar-nun, 1988; Rosenberg and Prialnik, 2009), and that this dust is primarily silicate in composition (Agarwal et al., 2007), we have used the secondary emission parameters reported by Tiersch and Notni (1989) for silicates ($E_{\max}$=420 eV and $\delta_{\max}$=2.5). Recent in-situ measurements of the secondary emission yield of lunar regolith using Lunar Prospector data have revealed that the effective yield is a factor of $\sim 3\times$ lower than what was expected from laboratory studies, possibly due to surface roughness effects (Halekas et al., 2009). It is plausible that a similar reduction may apply to the surface of 67P and therefore we have also included results for a lunar-like reduced secondary emission yield.

The photoelectron and secondary electron distributions are assumed to be Maxwellian, with temperatures of 2 eV and 3 eV, respectively. The normal electric field at the surface of the nucleus is given by $E_{\text{normal}} \sim \varphi_{\text{surface}}/\lambda_D$ (Mendis et al., 1981), where λ_D on the positive dayside nucleus depends on a combination of the ambient plasma and photoelectron Debye lengths as given by Stubbs et al. (2014)

$$\lambda_D = \sqrt{\frac{\varepsilon_0 k_B T_{\text{photoelectron}}}{e^2[n_{\text{photoelectron}} + n_{\text{electron}}(T_{\text{photoelectron}}/T_{\text{electron}}]}}$$

while for negatively charged and shadowed regions of the nucleus λ_D is simply given by $\lambda_D = \sqrt{\frac{\varepsilon_0 k_B T_{\text{electron}}}{n_{\text{electron}} e^2}}$. For the purpose of this study, we assume that the electrostatic potential above the nucleus decreases monotonically between the surface and the ambient plasma.

2.2. Comet plasma wake and surface charging of the nightside nucleus

During periods of low outgassing activity, the nucleus can be considered a simple plasma-absorbing obstacle to the solar wind flow. This absorption leads to a plasma void immediately downstream of the nucleus. Given the pressure gradient between the undisturbed plasma and the void, the ambient solar wind plasma will expand to fill this void. It has been shown that this process may, under certain conditions, be approximated by a 1-D self-similar solution for the expansion of a quasi-neutral non-magnetized plasma into a vacuum (Gurevich et al., 1969; Samir et al., 1983). Using a single Kappa distribution to describe solar wind electrons, Halekas et al. (2005) utilized one such solution for the lunar wake and found a geometric-like decrease in plasma density and a linear-like increase in electron temperature with increasing distance from the wake flank, with the latter arising from velocity filtration effects driven by the electric field that maintains quasi-neutrality. For cases with comparable ion and electron temperatures, the ion temperature can also be important in controlling the expansion, as discussed in detail by Halekas et al. (2014) for the case of the lunar wake. Building on the previous work of Halekas et al. (2005, 2014), we have modeled the plasma wake of the 67P nucleus as a cylindrically symmetric ion sonic expansion of an unmagnetized plasma into a vacuum, utilizing a 1-D numerical solution for finite-temperature ions and electrons, assuming quasi-neutrality (Halekas et al., 2014). Note that the quasi-neutrality assumption can be broken in small regions (such as the near-surface sheath), but even

the small 67P nucleus is large compared to the Debye scale, so we expect that this formulation should remain valid on the scale of the wake, as it does at the Moon. Previous work has shown that solar wind electrons may be adequately described by a single Kappa function (Maksimovic et al., 1997a, 1997b). However, due to the variable nature of the suprathermal component, realistic values of κ in the solar wind have been found to range from 2 to 5 (Zouganelis, 2008). Therefore, we consider the case of a fairly typical κ value of 4.5 and a more suprathermal case of $\kappa=3.0$. The ions are assumed to have a convecting Maxwellian distribution. Fig. 2 shows the resulting electron temperature and plasma density near the nucleus from our self-similar model for these two κ distributions. It should be emphasized that the exact values for the electron temperature and plasma density beyond SZA $\sim 110^\circ$ depend strongly on the suprathermal tails of the solar wind electron and ion distributions, which may not be well approximated by simple Kappa and Maxwellian distributions. What is clear, however, is that we may expect greatly enhanced electron temperatures of more than an order of magnitude within the cometary plasma wake, which has strong implications for the predicted surface potential on the nightside nucleus.

For a plasma with the electron component described by a Kappa distribution, the electron current to the surface of the nucleus becomes

$$J_0 = n_{\text{plasma}} q \sqrt{\frac{kT_\kappa}{2\pi m_{\text{electron}}}} \frac{\sqrt{\kappa - 3/2}\,\Gamma(\kappa - 1)}{\Gamma(\kappa - 1/2)}$$

and for a negatively charged surface with a potential φ_{surface}, the electron current becomes (Halekas et al., 2009).

$$J = J_0 \left(1 + \frac{q\varphi_{\text{surface}}}{(\kappa - 3/2)kT_\kappa}\right)^{1-\kappa}$$

2.3. Electrostatic dust levitation and ejection

As pointed out by Singer and Walker (1962), an individual dust grain of radius a lying on a surface with charge density σ will attain a charge that is proportional to its surface area

$$q_{\text{grain}} = \pi a^2 \sigma = a^2 \frac{E_{\text{normal}}}{4} = \frac{a^2 \varphi_{\text{surface}}}{4\lambda_D},$$

And as pointed out by Mendis et al. (1981) this implies that small grains (< 10 μm) will have an excess charge $N = q_{\text{grain}}/\text{e}$ which is $\ll 1\text{e}$. As grains cannot hold a fractional charge, they interpret this such that only a small fraction N of the grains on the surface will carry a charge of 1e. These grains may then be electrostatically lifted and levitated above the surface if the electrostatic force $F_e = q_{\text{grain}} E_{\text{normal}}$ exceeds the gravitational force F_g, assuming that any cohesive forces are negligible. This yields a critical grain radius $a_{\text{levitation}}$ below which the grains may be electrostatically levitated (Flammer et al., 1986; Lee, 1996; Mendis et al., 1981)

$$a_{\text{levitation}} = \sqrt[3]{\frac{q_{\text{grain}} |E_{\text{normal}}|}{2G\pi^2 R_{\text{nucleus}} \rho_{\text{nucleus}} \rho_{\text{grain}}}}.$$

Similarly, dust grains that are much smaller than $a_{\text{levitation}}$ may be immediately ejected from the surface and escape the gravitational potential of the nucleus if the total energy $q_{\text{grain}} |\varphi_{\text{surface}}| - GM_{\text{nucleus}} m_{\text{grain}}/R_{\text{nucleus}} > 0$, yielding a second critical grain radius a_{escape} (Lee, 1996; Mendis et al., 1981)

$$a_{escape} = \sqrt[3]{\frac{q_{grain} |\varphi_{surface}|}{2G\pi^2 R^2_{nucleus} \rho_{nucleus} \rho_{grain}}}.$$

For the purpose of our calculations, we assume that the mean effective radius of the nucleus is 2 km and that the bulk density of the nucleus and dust particles is $0.4\ \text{g/cm}^3$ and $1\ \text{g/cm}^3$, respectively.

2.4. Flux of ejected charged nanodust from the surface

In the case of an active comet, the emitted neutral gas is capable of lifting and emitting dust grains from the surface (e.g. Agarwal et al., 2007). This is expected to be the case even for the weakly outgassing nucleus of comet 67P when it is at relatively large comet–Sun distances of ~ 3 AU (Snodgrass et al., 2013; Tenishev et al., 2011, 2008). Submicron dust grains have been observed in-situ around comet Halley by the Giotto and the Vega 1 and 2 spacecraft and it was estimated that attogram (10^{-18} g) grains accounted for several percent of the total dust emission from the comet (Sagdeev et al., 1989; Utterback and Kissel, 1990). This implies that a large fraction of the dust emitted from the nucleus was in the form of submicron dust grains. It is similarly expected that comet 67P will be a significant source of submicron dust particles (Szego et al., 2014; Tenishev et al., 2011; Vigren et al., 2015). Once they are lifted from the surface, the small fraction of submicron grains which carry an electric charge may be freely accelerated by near-surface electric fields. Therefore the flux of charged submicron dust particles emitted from the surface of the nucleus depends on both electrical (e.g. surface charging) as well as neutral (gas production) effects.

In order to estimate the rate of gas emission at a given SZA we have made use of the H_2O gas emission profiles for comet 67P calculated by Tenishev et al. (2008). Based on observations made by the Rosetta MIRO instrument, Gulkis et al. (2015) reported a total water production rate of 4×10^{25} molecules/s when the comet was at a comet–Sun distance of 3.4 to 3.6 AU. In order to obtain the gas emission profile at ~ 3.5 AU, we therefore scale the total water production rate calculated by Tenishev et al. (2008) to this observed value. For the lander touchdown at ~ 3 AU, we scale the total water production rate of Gulkis et al. (2015) using a scaling factor of $R^{5.9}$ as suggested by Snodgrass et al. (2013). The production of CO is assumed by be proportional to that of H_2O at a level of 5%, as given by Tenishev et al. (2008). Similarly, the production of CO_2 is assumed to proportional to that of H_2O, with a CO_2/H_2O ratio of 52% at 3.5 AU and 21% at 3 AU, respectively (Snodgrass et al., 2013).

Additionally, to provide some quantifiable prediction of submicron dust emission from the nucleus, we must first know the ratio between the gas and dust emission rates at the surface. For submicron dust particles, this ratio is currently not well constrained and the exact distribution of emitted cometary submicron grains is not known. Vigren et al. (2015) performed modeling of nanograin emission from the nucleus of comet 67P and considered the case of 2 nm dust grains with a dust to gas ratio of $\sim 1\%$. These authors argued that while considerable uncertainty still exists, these values at least appear to be compatible with the in-situ measurements of submicron dust at comet Halley (Sagdeev et al., 1989; Utterback and Kissel, 1990) as well as, by analogy, with the nanodust observed in the Enceladus Plume by Cassini (Hill et al., 2012; Jones, 2012; Jones et al., 2009). Thus, in order to provide an order-of-magnitude estimate of the flux of charged submicron dust from the nucleus, we consider the emission of charged nanograins with a typical radius of 2 nm and adopt the dust to gas ratio suggested by Vigren et al. (2015).

In order to calculate the flux of charged nanograins from the surface, we follow the same general approach as outlined in Szego et al. (2014). First we consider the timescale for a given dust grain to attain a charge of 1e, given by $t_{\text{ch}} \sim \text{e}/I_{\text{grain}}$, where I_{grain} is proportional to the surface area of the grain. The probability that a given dust grain attains a charge of $(\pm)1\text{e}$ over an intervall Δt is therefore $p_{\text{ch}} \approx \Delta t/t_{\text{ch}}$. The flux of emitted charged nanograins at

the surface is then given by

$$F_{ch} = \frac{F_{gas} f_{dust}}{m_{grain}} p_{ch}$$

where F_{gas} is the gas mass flux, f_{dust} is the ratio of dust to gas and m_{grain} is the mass of a spherical dust grain with radius 2 nm.

3. Results

3.1. Surface potential

Shown in Fig. 3 are our model results at a comet–Sun distance of 3.5 AU, which is applicable to the Rosetta rendezvous. On the dayside nucleus, the predicted surface potential reaches a maximum of +5.8 V at the subsolar point and slowly decreases until a zero crossing at a Solar Zenith Angle (SZA) of ~84°. Beyond this point, the surface potential grows increasingly negative, reaching −15 V at the sunlight terminator (SZA 90°). Within the plasma wake region (SZA > 90°), the electron temperature rises roughly linearly from the wake flank, reaching 230 eV and 77 eV near the center of the wake (SZA 180°) for κ values of 3.0 and 4.5, respectively. These predicted values are somewhat higher than those derived (and observed) for the Moon, largely because of the higher ion Mach number assumed at greater distances from the Sun, which makes it more difficult for plasma to access the shadowed surface in the wake. Similarly, the plasma density decreases roughly exponentially within the wake, reaching a reduction of ~5 to 6 orders of magnitude compared to ambient values near the center of the wake. The surface potential within the wake grows increasingly negative with increasing SZA, reaching nearly −400 V and −300 V for κ values of 3.0 and 4.5. However, for both chosen values of κ, the surface potential becomes positive towards the center of the wake. This is due to the increasingly large electron temperature there, which leads to a secondary electron emission yield that exceeds unity, and thus the surface charges towards a slightly positive potential. In the case of a reduced secondary emission yield due to surface roughness effects (c.f. Halekas et al., 2009), the predicted surface potential becomes increasingly more negative towards the center of the wake, reaching more than −2 kV in the case of κ= 3.0 and −600 V in the case of κ=4.5. Model predictions for the nucleus during the time of the Philae landing at ~3 AU are shown in Fig. 4, but as the results are relatively similar to those of the rendezvous case, they will not be discussed further.

3.2. Electrostatic dust acceleration above the nucleus

As shown in Fig. 3, dust grains with radii below ~50 nm may be electrostatically ejected from the nucleus on the dayside. Near the solar terminator, grains with radii < 0.1 μm may be ejected, while increasingly larger grains may be ejected as we move towards the center of the wake, as the surface potential grows

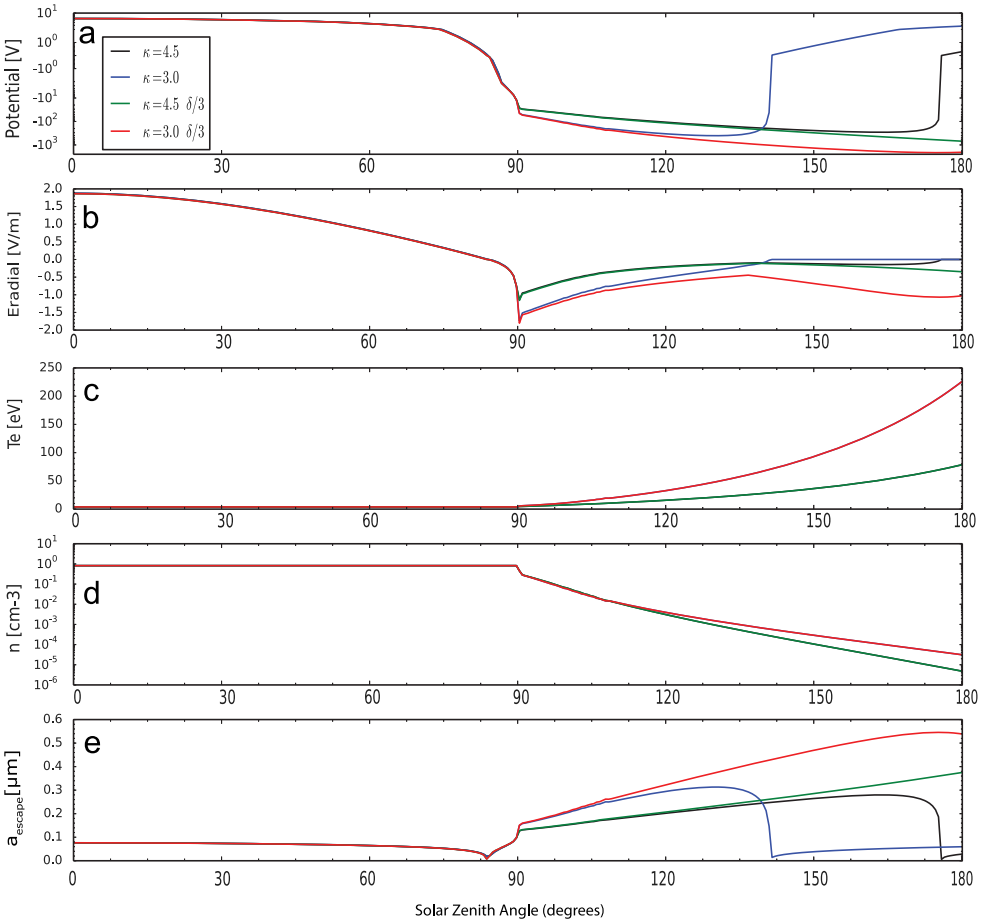

Fig. 3. Model results for Rosetta's initial rendezvous with comet 67P at 3.5 AU shown in black and blue are the model results for solar wind electron κ values of 3 and 4.5 assuming a nominal secondary emission yield. Shown in red and green are the same cases but assuming a reduced secondary emission yield. Panels (a) and (b) show the calculated surface potential and normal electric field, respectively. Panels (c) and (d) show the electron temperature and density as calculated using the self-similar model. Panel (e) shows the critical (maximum) radius for a dust grain to be electrostatically ejected from the nucleus. (For interpretation of the references to color in this figure legend, the reader is referred to the web version of this article.)

increasingly negative. In the case of a reduced secondary emission yield, dust grains as large as 0.4–0.5 μm may be ejected from the nucleus near the center of the wake, depending on the value of κ. For comparison, dust grains with radii as large as $\sim$0.5 μm may in principle be electrostatically levitated at some height above the dayside nucleus at SZA $<60^\circ$ and near the terminator. However, modeling the behavior of these levitated grains is more complex as they will also interact with their respective photoelectron/Debye sheaths. In the event that these larger grains attain additional charge within the sheath, they too may be capable of escaping the nucleus.

3.3. Flux of charged nanograins from the surface

Shown in Fig. 5 is the predicted rate of outgassing from the surface as well as the rate of charged nanograin emission. As can be seen, the rate of charged nanograin emission above the dayside nucleus is relatively well correlated with the gas production rate, with the highest emission rates at the subsolar point and slowly decreasing emission rate with increasing SZA. However in the near-terminator region and at the nightside nucleus the rate of charged nanograin emission drops by several orders of magnitude, reaching a value which is more than 5 orders of magnitude lower than that of the subsolar point at large SZAs. This can be explained by the fact that while the charging timescales above most of the dayside are dominated by the photoemission current, charging of the nightside nucleus is dominated by the comparatively weaker current due to the ambient plasma electrons. Thus the charged nanograin emission rate grows increasingly smaller towards the center of the wake as the ambient plasma density decreases drastically (c.f. Fig. 2). For the same reason, the chosen value of κ for the solar wind electrons has no impact on charged nanograin emission at the dayside and in the near-terminator regions but generally leads to higher emission rates for smaller values of κ as we move towards the center of the wake.

3.4. Free-floating grains far from the nucleus

For free-floating grains far from the nucleus, i.e. not embedded within the photoelectron/Debye sheath near the surface, we cannot utilize the sheath-limited formulation of Manka (1973) and therefore make use of the Orbit-Limited Motion approach developed for spherical probes in a plasma (e.g. Allen, 1992). In this case, the solar wind electron collection current onto a positively charged grain is given by (Horányi, 1996).

$$I_e = 4\pi a_{\mathrm{grain}}^2 n_{\mathrm{plasma}} \sqrt{\frac{kT_{\mathrm{electron}}}{2\pi m_{\mathrm{electron}}}} \left(1 + \frac{e\varphi_{\mathrm{grain}}}{kT_{\mathrm{electron}}}\right)$$

The potential on a small, sunlit, free-floating grain far from the nucleus is thus $\sim+4.5$ V. If we assume that these grains are

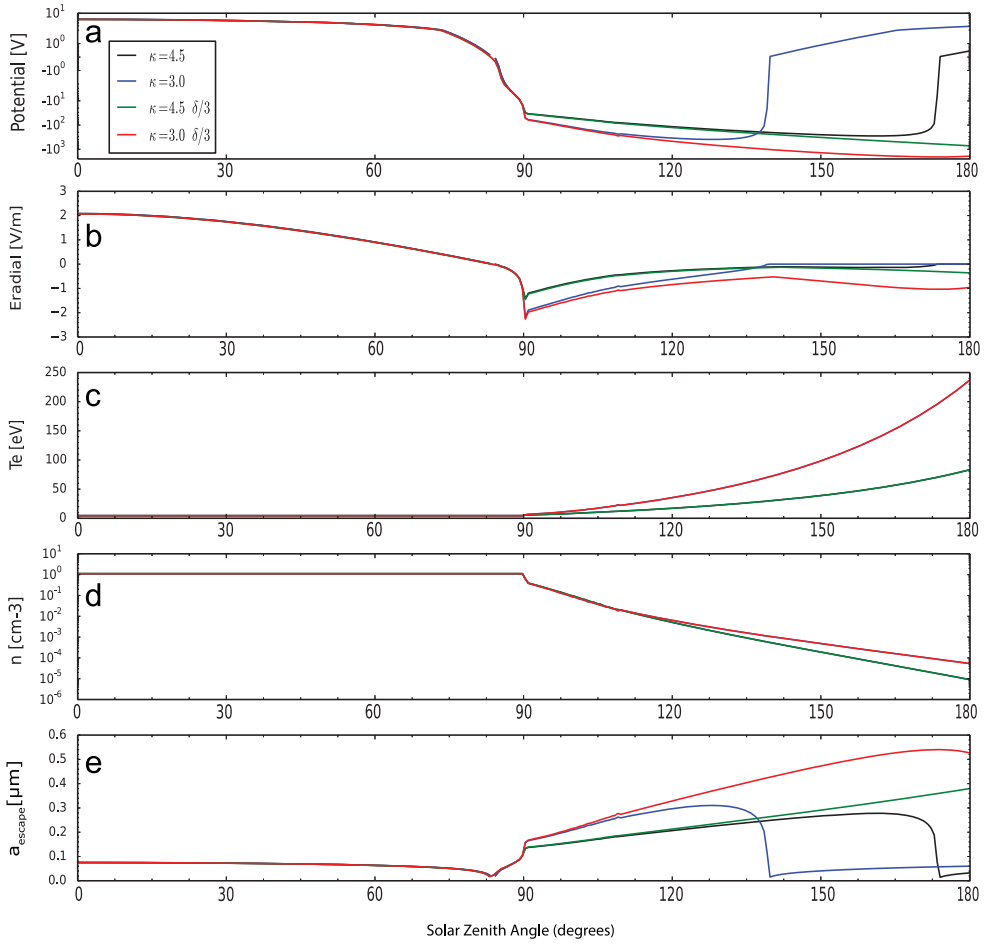

Fig. 4. Model results for 67P at 3 AU. Shown in black and blue are the model results for solar wind electron κ values of 3 and 4.5 assuming a nominal secondary emission yield. Shown in red and green are the same cases but assuming a reduced secondary emission yield. Panels (a) and (b) show the calculated surface potential and normal electric field, respectively. Panels (c) and (d) show the electron temperature and density as calculated using the self-similar model. Panel (e) shows the critical (maximum) radius for a dust grain to be electrostatically ejected from the nucleus. (For interpretation of the references to color in this figure legend, the reader is referred to the web version of this article.)

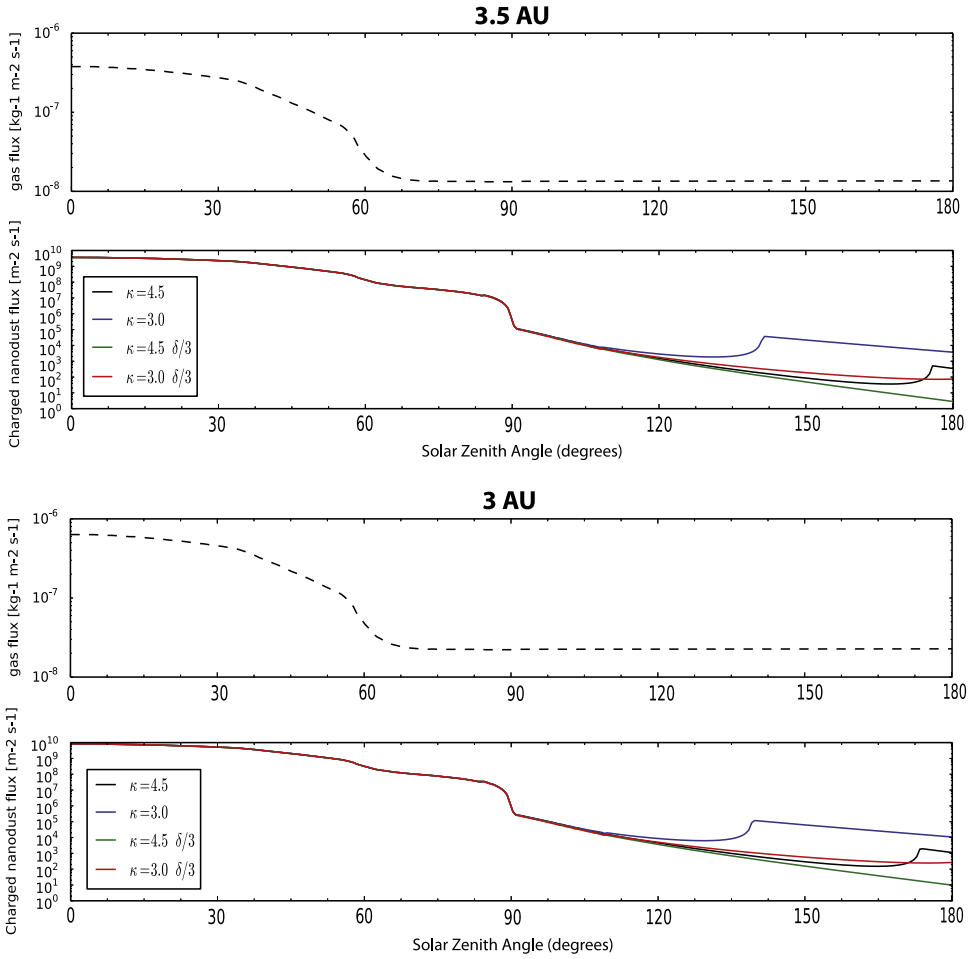

Fig. 5. Calculated rate of H2O, CO and CO_2 gas production from the surface (top) and the calculated flux of escaping charged nanodust at the surface (bottom) for comet 67P at comet–Sun distances of 3.5 AU and 3 AU.

spherical, then the equilibrium charge may be calculated such that $q_{\text{grain}} = 4\pi\varepsilon_0 a_{\text{grain}} \varphi_{\text{grain}}$ (e.g. Kempf et al., 2006). As shown in Fig. 6, a sunlit grain with radius 10 nm thus carries a charge of ~31e and a 100 nm grain carries a charge of ~310e.

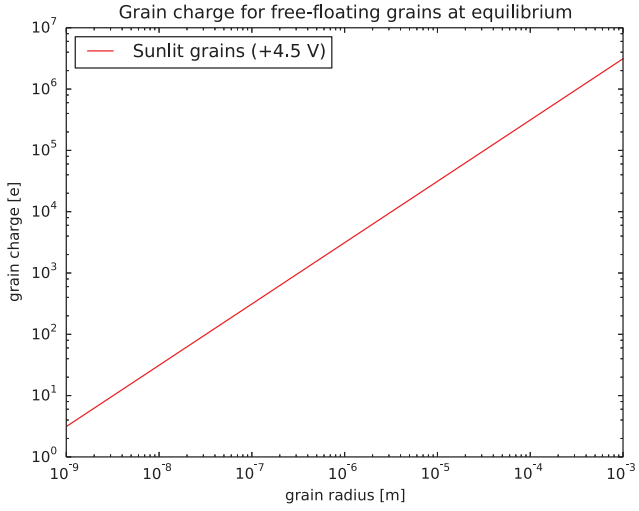

Fig. 6. Predicted equilibrium charge versus radius for free-floating dust grains far from the cometary nucleus.

4. Possible observations by Rosetta and Philae

4.1. Surface charging

The Rosetta spacecraft carries a complete suite of particle and fields instruments (Carr et al., 2007), including the Ion and Electron Sensor (IES), which is capable of detecting ions and electrons from 1 eV/e to 22 keV/e with an energy resolution $\Delta E/E$ of 4% (Burch et al., 2006). During times when the Rosetta spacecraft is magnetically connected to the nucleus, i.e. when an interplanetary magnetic field line connects the spacecraft to a point on the surface, the IES instrument may remotely detect surface charging on the nucleus by studying the interaction of solar wind electrons with the surface. In the case of an electrically neutral or positively charged surface, incoming solar wind electrons will simply be absorbed. As illustrated in Fig. 7, in the case of a negatively charged surface, electrons with energies below the surface potential will be electrostatically reflected, while secondary electrons near the surface may be accelerated up towards Rosetta by the potential difference between the surface and the spacecraft. The results shown in Figs. 3 and 4 indicate that we may expect such secondary electron beams to be generated from negatively charged regions near the terminator and on the nightside nucleus. By studying populations of upwards and downward-going electrons, surface potentials may be inferred by searching for field-aligned beams of secondary electrons as well as energy-dependent loss cones due to absorbed solar wind electrons which have sufficiently large energies such that they are not electrostatically reflected. These techniques have been employed successfully at the Moon

(e.g. Halekas et al., 2002, 2011) and at Saturn's moon Hyperion (Nordheim et al., 2014). Using the Electron Reflectometer instrument onboard the Lunar Prospector spacecraft, Halekas et al. (2009) has demonstrated the viability of performing in-situ measurements of secondary emission yields from lunar regolith using measurements of emitted secondary electrons. The instruments onboard Rosetta and Philae could similarly be used to perform in-situ characterization of secondary emission from negatively charged regions of the 67P nucleus, which may greatly aid future modeling efforts. At Saturn's moons Rhea (Santolík et al., 2011) and Hyperion (Nordheim et al., 2014), intense electrostatic wave activity has been associated with surface-originating electron beams. In the case of 67P, similarly associated electrostatic wave activity may be detectable by the Rosetta Mutual Impedance Probe (RPC-MIP) instrument (Trotignon et al., 2006) where surface-originating electron beams are present.

The Philae lander carries a low energy electron and ion instrument, ROMAP-SPM and a magnetometer, ROMAP-ROMAG (Auster et al., 2007), and may therefore be capable of detecting in-situ surface charging conditions at its landing site, which will be located within the photoelectron or Debye sheath, depending on the local illumination conditions. Thus, there is significant potential for synergistic science using both the Rosetta spacecraft and Philae. Importantly, remote measurements of surface charging by RPC–IES may be compared to the in-situ measurements of the near surface environment made by ROMAP, which will provide important context as well as the potential for "ground truth". At the time of writing, the Philae landing has occurred, but the scientific results from the surface have not yet been published. Furthermore, while the initial operational lifetime of the lander was shorter than expected, the possibility remains that it may be reactivated in the future, possibly allowing for further comparison between model results and observation, for example given an extended post-perihelion mission.

4.2. Charged submicron dust

We have shown that dust grains with radii <50 nm may be electrostatically ejected from most of the dayside, and that near the terminator and on the night side, grains <0.4–0.5 μm may be ejected. The Rosetta spacecraft carries several instruments capable of detecting cometary dust, including GIADA (Colangeli et al., 2007) and COSIMA (Kissel et al., 2007). GIADA is capable of detecting the size, velocity distribution and mass of dust grains larger than ~ 10 μm while COSIMA provides information on the composition of dust grains in the ~ 10 to 100 μm size range. Thus, it is clear that the dust instruments on the Rosetta orbiter are not capable of detecting charged submicron dust particles which are emitted from the nucleus. However, as pointed out by Szego et al. (2014), the RPC–IES instrument, while not designed to study dust, may be capable of directly detecting charged nanograins which are ejected from the nucleus. Previously, a similar instrument, the Cassini Electron Spectrometer (ELS), part of the Cassini Plasma Spectrometer (CAPS) has been used to directly observe charged nanograins in the Enceladus plume (Jones et al., 2009). Here we assume that the acceleration due to gas drag on the nanograin particles is negligible compared to that of electrostatic forces, and thus the kinetic energy of the charged nanograins should reflect the surface potential at the region of the nucleus from which they are emitted (e.g. Szego et al., 2014). For grains with radii $\ll a_{\mathrm{escape}}$, the observed kinetic energy of the grain will be $E_k \sim q_{\mathrm{grain}} |\varphi_{\mathrm{surface}}|$, thus yielding energies that are detectable by RPC–IES for charged nanograins emitted from most SZAs, except near the predicted zero-crossing at SZA $\sim 84^\circ$, where we expect a dust "dead zone" due to the very small surface potentials present.

Using the calculated flux of charged nanograins emitted from the surface of the nucleus we may estimate the charged nanograin flux at the Rosetta orbiter for a given altitude above the surface by R^{-2} where $R = R_{\mathrm{orbiter}}/R_{\mathrm{nucleus}}$. Furthermore, if we assume that the RPC–IES instrument is nadir-pointing, the effective nanograin collection area is 1.4 cm^2 (Szego et al., 2014). The RPC–IES instrument was not calibrated for charged nanograins, and thus, the detection efficiency for such particles is not currently known. However, based on the laboratory studies of Fraser (2002), we adopt an efficiency factor of 5%, similar to that previously used for charged nanograins (Hill et al., 2012) and heavy negative ions (Coates et al., 2009, 2007; Wellbrock et al., 2013) detected by the CAPS–ELS instrument onboard Cassini. Shown in Fig. 8 are the predicted count rates in the RPC–IES instrument due to charged

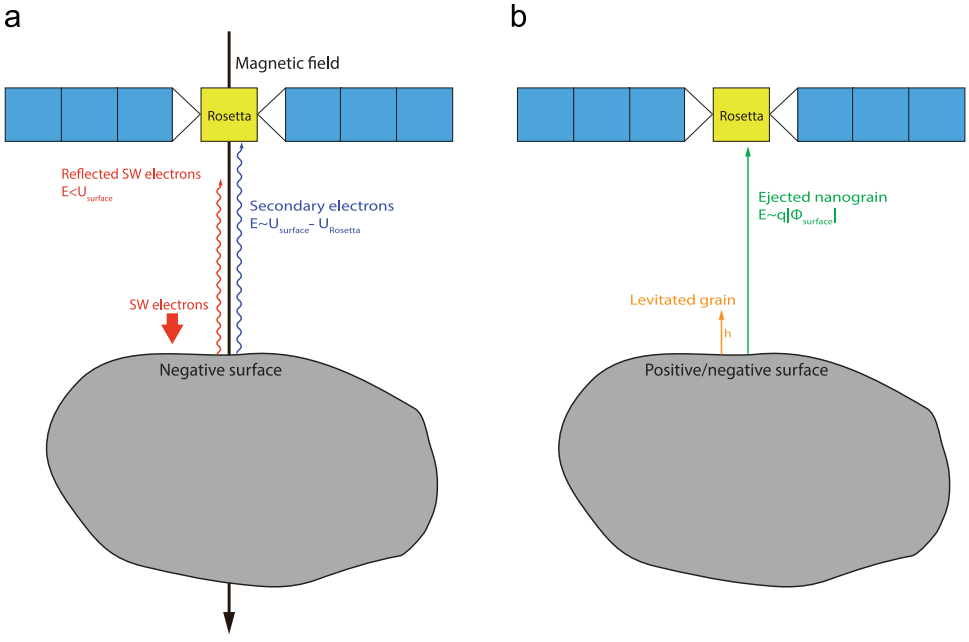

Fig. 7. Illustration showing (a) how Rosetta may perform remote sensing of negatively charged surfaces on the nucleus and (b) how ejected charged nanograins may be detected in-situ by RPC–IES.

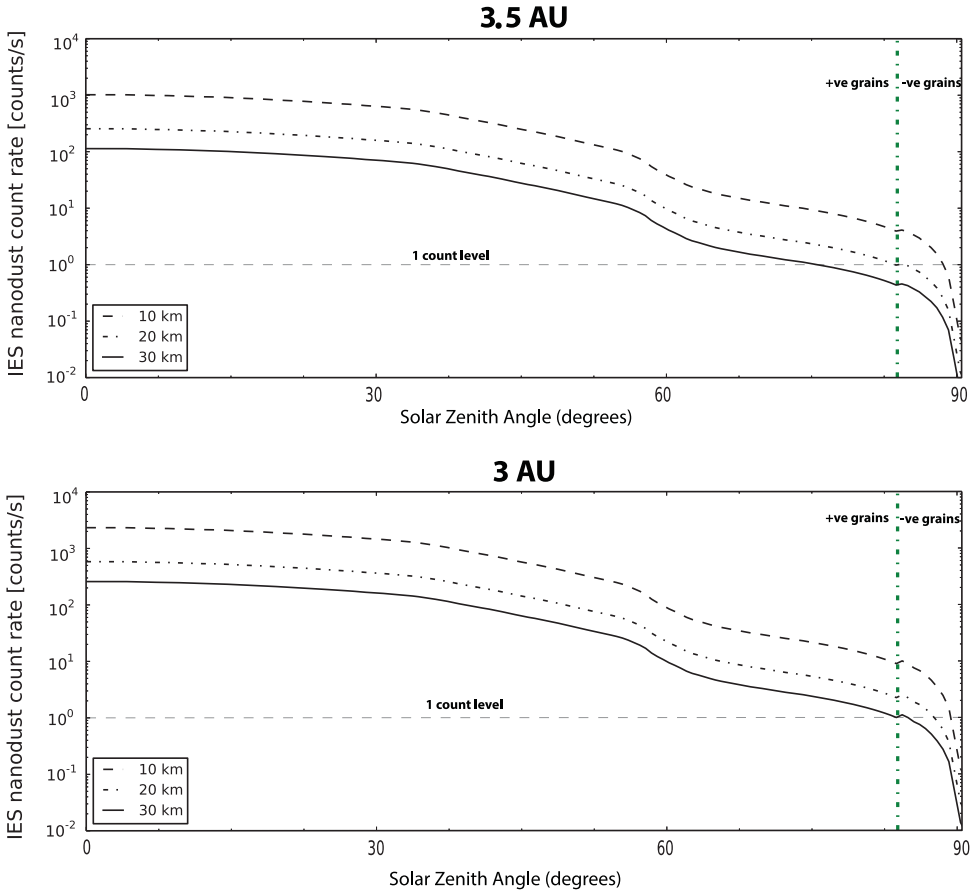

Fig. 8. Calculated count rate in the RPC–IES instrument due to charged nanodust at orbiter altitudes of 10, 20 and 30 km. The dashed horizontal bar shows the instrument one count level and the dashed vertical line shows the transition from positively to negatively charged grains.

nanograins for orbiter altitudes of 10, 20 and 30 km. The flux of charged nanograins emitted from the nightside nucleus is too low to be detected at any SZA and therefore only the results for the dayside are shown here. As can be seen, the charged nanograins emitted from the dayside surface yield a detectable flux at the orbiter, reaching on the order of $\sim 10^2$ to 10^3 counts/s at the subsolar point and slowly decreasing to the one-count level at the terminator. A significant day-to-night variation in observations of charged nanograins is therefore expected, with high count rates above the subsolar point and no observable signal above the noise level above the night side nucleus. Furthermore, while the charged dust grains emitted from the dayside nucleus will be positively charged, a cross-over from positively to negatively charged dust grains is expected to occur at SZA $\sim 84°$, with negatively charged grains emitted from near-terminator regions. In the context of orbiter observations we would therefore expect to encounter a population of negatively charged nanograins when the spacecraft crosses above the local terminator.

In addition, the Philae lander carries the SESAME-DIM instrument, which is capable of detecting grains with radii $> 0.5\ \mu m$ (Biele and Ulamec, 2007) and could therefore feasibly be sensitive to electrostatically mobilized dust grains near the surface. While such grains may not necessarily be electrostatically ejected from the nucleus, they may nonetheless be levitated and experience horizontal motion due to local electric field gradients. At the Moon, a similar effect has been attributed to greatly enhanced dust flux detected near local sunset and sunrise as observed by the Apollo LEAM instrument (Berg et al., 1976).

5. Discussion

The model predictions presented herein are given as a function of SZA, i.e. as a function of the angle to the incoming solar UV and solar wind flow. Recent imaging of the 67P nucleus by Rosetta has revealed a highly non-spherical object with a double-lobe type structure (Sierks et al., 2015; Thomas et al., 2015). Thus, as illustrated in Fig. 1, the results for a given SZA may be applicable to multiple points on the surface. Similarly, local surface topography may lead to shadowing from solar UV and inflowing solar wind plasma, leading to the formation of "mini-wakes". Previous investigations of such local shadowing effects on the Moon (e.g Farrell et al., 2007) and on small (~ 100 m) double-lobed near-Earth asteroids (Zimmerman et al., 2014) have found that large negative potentials, similar to those found at the night side, may develop in locally shadowed regions. On 67P, this is particularly applicable to the "neck" which connects the two lobes of the nuclei, which may in certain rotational configurations be shadowed from solar UV and the solar wind flow. Under such conditions, we may therefore expect this region to reach significant negative potentials, on the order of the predicted surface potentials in the near-terminator regions of the downstream nucleus (< -15 V). Under certain conditions, the locally shadowed neck may also be exposed to reflected solar UV from sunlit areas elsewhere on the nucleus. If we consider a typical cometary albedo of 4%, such regions may be expected to reach slightly positive potentials of up to a few volts positive if the reflected sunlight impinges along the local zenith.

It has been proposed that strong multipole electric fields may occur at sunlight-shadow boundaries due to high energy (~50 to 500 eV) photoelectrons emitted from sunlit areas subsequently striking adjacent shadowed regions (Criswell and De, 1977; De and Criswell, 1977). At centimeter-sized spatial scales, De and Criswell (1977) have shown that local electric fields in excess of $2E_{\text{photoelectron}}\,[V/cm]$ may be generated across adjacent sunlit and shadowed regions. Strong small-scale electric fields on the order of ~100 to 1000 V/cm could therefore exist in regions near the terminators and at local sunlit-shadow boundaries on planetary objects of low resistivity. In the case of a rotating body, Lee (1996) has shown that the terminator crossing time (and thus time available for charging) is a possible constraint for this process. However, for a relatively slowly rotating body like the 67P nucleus, with a rotational period of ~12 h, this does not preclude such levels of charging from occurring. Shadowing due to the topography of the 67P nucleus may therefore be associated with strong electric fields on the order of ~100–1000 V/cm over centimeter scales. Such locally enhanced electric fields may lead to increased rates of electrostatic dust ejection and possibly also to motion of charged grains across shadow boundaries due to strong local electric field gradients. While such illumination conditions are certainly present near the terminators, imaging of the 67P nucleus has revealed an object with rugged small-scale topography (Thomas et al., 2015). Thus, we may also expect to see similarly enhanced local small scale electric fields due to shadowing from boulders, escarpments and crater rims.

In the present work we have assumed that the electrostatic potential in the photoelectron sheath above illuminated regions decreases monotonically between the surface and the ambient plasma. However, several authors have shown that a non-monotonic solution also exists for the photoelectron-sheath (Guernsey and Fu, 1970; Nitter et al., 1998; Poppe and Horányi, 2010), and recent observations confirm that these potential structures occur on the Lunar dayside (Halekas et al., 2008; Poppe et al., 2012b) for some plasma conditions (e.g. the Moon in Earth's magnetotail). Recent 1-D and 3-D particle-in-cell simulations of the Moon in the solar wind do not predict non-monotonic potentials in the dayside photoelectron sheath (Kallio et al., 2012; Poppe et al., 2012a), although it should be noted that these studies may have been limited by the choice of simulation dimensions (Stubbs et al., 2014). Similarly, for a cometary nucleus at 3 AU, Juhász and Szegő (1998) did not predict the formation of a non-monotonic photoelectron sheath. Thus, our choice of a monotonic sheath is likely a reasonable assumption. However, if a non-monotonic sheath was indeed present above the dayside nucleus, a negative potential may form within the sheath at some distance above the surface. Importantly, this negative potential may act to trap photoelectrons near the surface and may allow for acceleration of cold photoelectrons up towards the spacecraft due to the potential difference at times of magnetic connection. In addition to possible in-situ observations of the photoelectron sheath by Philae, the detection of such photoelectron beams and energy-dependent loss cones above illuminated surfaces by RPC–IES would be a clear indication that the structure of the photoelectron sheath is non-monotonic. It is not expected that a non-monotonic sheath profile would greatly affect the surface potential on the dayside (e.g. Stubbs et al. 2014) and recent work by Aplin et al. (2014) has shown that the type of sheath structure has negligible effect on the photoelectron density near the surface. In the context of electrostatic effects on dust grains, a non-monotonic sheath profile would also lead to the presence of a downward directed electric field within the sheath, which would act to decelerate charged grains ejected from the surface. However, as noted by Poppe and Horányi (2010), such effects would not necessarily preclude dust levitation and lofting from occurring.

Here we have assumed that the acceleration of charged nanograins due to gas drag is negligible compared to the acceleration by electrostatic forces. This is consistent with the predictions of Tenishev et al. (2011), who presented velocity and size distributions for emission of larger submicron grains at comet 67P. However, it should be noted that the emission of nanometer-sized grains has not been explicitly studied in the existing literature. If the nanograins were instead emitted with a velocity comparable to that of the bulk gas flow, as recently assumed by Vigren et al. (2015), the observed kinetic energy of charged nanograins at the orbiter would be significantly higher than what the surface potential at the nucleus would suggest. If we consider a radial gas velocity of ~500 m/s (Tenishev et al., 2008), the resulting kinetic energy for charged nanograins of radius 2 and 20 nm would be, ~26 eV and ~26 keV, respectively. This would not alter the predicted flux of charged nanograins at the orbiter as shown in Fig. 8. However, if the charged nanograin population was observed to extend to such high energies, this would be a strong indication that gas drag dominates over electrostatic forces in the vicinity of the nucleus.

6. Summary

Here we have presented modeling of surface charging of the 67P nucleus during periods of low outgassing activity for typical solar wind conditions. As shown, illuminated areas of the nucleus can be expected to reach a slightly positive potential at most SZAs, with a predicted potential of ~+6 V at the subsolar point. We have also presented the results of a self-similar model of the cometary plasma wake, showing that significantly enhanced electron temperatures may be expected at the nightside nucleus, leading to strongly negative surface potentials on the order of −300 to −400 V in certain regions. As the electron temperature increases towards the center of the wake, the secondary emission yield exceeds unity and the surface rapidly approaches a slightly positive surface potential. We have also explored the consequences of a lunar-like, reduced secondary emission yield, which allows the nightside nucleus to reach very large negative potentials, in the range of −600 V to ~−2 kV near the wake center.

We have shown that charged dust grains with radii <50 nm may be electrostatically ejected from the nucleus at most SZAs. Using profiles of the cometary outgassing rate at the surface scaled to the actual observations of cometary activity by Rosetta, we have provided an estimate for the flux of charged nanograins (a_{grain} ~2 nm) that are emitted from the surface. While these dust particles are too small to be observed by the dust instruments on the Rosetta orbiter, we have shown that the flux of charged nanograins above the dayside and near-terminator nucleus is sufficiently high to be detected by the RPC–IES instrument. We have also shown that the flux of charged nanograins from the shadowed areas within the comet's plasma wake is insufficient to yield a significant count rate in RPC–IES instrument.

Acknowledgments

We wish to thank the UCL Graduate School for funding which enabled TAN to contribute to this research. This work was carried out by members of the "Kinetic processes at airless bodies" team supported by the International Space Science Institute (ISSI).

References

Agarwal, J., Müller, M., Grün, E., 2007. Dust environment modelling of comet 67P/Churyumov-Gerasimenko. Space Sci. Rev. 128, 79–131. http://dx.doi.org/10.1007/s11214-006-9139-1.

Allen, J.E., 1992. Probe theory-the orbital motion approach. Phys. Scr. 45, 497–503. http://dx.doi.org/10.1088/0031-8949/45/5/013.

Aplin, K.L., Macfaden, A.J., Bowles, N.E., 2014. Modelling of an asteroid photoelectron sheath and implications for a sample return mission. Planet. Space Sci. 99, 103–111. http://dx.doi.org/10.1016/j.pss.2014.04.018.

Auster, H.U., Apathy, I., Berghofer, G., Remizov, A., Roll, R., Fornacon, K.H., Glassmeier, K.H., Haerendel, G., Hejja, I., Kührt, E., Magnes, W., Moehlmann, D., Motschmann, U., Richter, I., Rosenbauer, H., Russell, C.T., Rustenbach, J., Sauer, K., Schwingenschuh, K., Szemerey, I., Waesch, R., 2007. ROMAP: Rosetta Magnetometer and Plasma Monitor. Space Sci. Rev. 128, 221–240. http://dx.doi.org/10.1007/s11214-006-9033-x.

Berg, O.E., Wolf, H., Rhee, J., 1976. Lunar soil movement registered by the apollo 17 cosmic dust experiment. In: Elsässer, H., Fechting, H. (Eds.), Interplanetary Dust and Zodiacal Light, Lecture Notes in Physics. Springer Berlin Heidelberg, Berlin, Heidelberg, pp. 233–237. http://dx.doi.org/10.1007/3-540-07615-8.

Biele, J., Ulamec, S., 2007. Capabilities of Philae, the Rosetta lander. Space Sci. Rev. 138, 275–289. http://dx.doi.org/10.1007/s11214-007-9278-z.

Biermann, L., Brosowski, B., Schmidt, H.U., 1967. The interaction of the solar wind with a comet. Sol. Phys. 1, 254–284. http://dx.doi.org/10.1007/BF00150860.

Brin, G.D., Mendis, D.A., 1979. Dust release and mantle development in comets. Astrophys. J. 229, 402–408. http://dx.doi.org/10.1086/156966.

Burch, J.L., Goldstein, R., Cravens, T.E., Gibson, W.C., Lundin, R.N., Pollock, C.J., Winningham, J.D., Young, D.T., 2006. RPC-IES: the Ion and Electron Sensor of the Rosetta Plasma Consortium. Space Sci. Rev. 128, 697–712. http://dx.doi.org/10.1007/s11214-006-9002-4.

Carr, C., Cupido, E., Lee, C.G.Y., Balogh, A., Beek, T., Burch, J.L., Dunford, C.N., Eriksson, A.I., Gill, R., Glassmeier, K.H., Goldstein, R., Lagoutte, D., Lundin, R., Lundin, K., Lybekk, B., Michau, J.L., Musmann, G., Nilsson, H., Pollock, C., Richter, I., Trotignon, J.G., 2007. RPC: the Rosetta Plasma Consortium. Space Sci. Rev. 128, 629–647. http://dx.doi.org/10.1007/s11214-006-9136-4.

Coates, A.J., Crary, F.J., Lewis, G.R., Young, D.T., Waite, J.H., Sittler, E.C., 2007. Discovery of heavy negative ions in Titan's ionosphere. Geophys. Res. Lett., 34; , pp. 6–11. http://dx.doi.org/10.1029/2007GL030978.

Coates, A.J., Wellbrock, A., Lewis, G.R., Jones, G.H., Young, D.T., Crary, F.J., Waite, J.H., 2009. Heavy negative ions in Titan's ionosphere: altitude and latitude dependence. Planet. Space Sci., 57; , pp. 1866–1871. http://dx.doi.org/10.1016/j.pss.2009.05.009.

Coates, A., 1997. Ionospheres and magnetospheres of comets. Adv. Space Res. 20, 255–266.

Coates, A.J., 2004. Ion pickup at comets. Adv. Space Res. 33, 1977–1988. http://dx.doi.org/10.1016/j.asr.2003.06.029.

Colangeli, L., Lopez-Moreno, J.J., Palumbo, P., Rodriguez, J., Cosi, M., Corte, V.Della, Esposito, F., Fulle, M., Herranz, M., Jeronimo, J.M., Lopez-Jimenez, A., Epifani, E. M., Morales, R., Moreno, F., Palomba, E., Rotundi, A., 2007. The Grain Impact Analyser and Dust Accumulator (GIADA) experiment for the Rosetta Mission: Design, Performances and First Results. Space Sci. Rev. 128, 803–821. http://dx.doi.org/10.1007/s11214-006-9038-5.

Cravens, T.E., Gombosi, T.I., 2004. Cometary magnetospheres: a tutorial. Adv. Space Res. 33, 1968–1976. http://dx.doi.org/10.1016/j.asr.2003.07.053.

Criswell, D.R., De, B.R., 1977. Intense localized photoelectric charging in the lunar sunset terminator region, 2. Supercharging at the progression of sunset. J. Geophys. Res. 82, 1005–1007. http://dx.doi.org/10.1029/JA082i007p01005.

De, B.R., Criswell, D.R., 1977. Intense localized photoelectric charging in the lunar sunset terminator region, 1. Development of potentials and fields. J. Geophys. Res. 82, 999–1004. http://dx.doi.org/10.1029/JA082i007p00999.

Farrell, W.M., Stubbs, T.J., Vondrak, R.R., Delory, G.T., Halekas, J.S., 2007. Complex electric fields near the lunar terminator: The near-surface wake and accelerated dust. Geophys. Res. Lett. 34, L14201. http://dx.doi.org/10.1029/2007GL029312.

Flammer, K.R., Jackson, B., Mendis, D.A., 1986. On the brightness variations of comet Halley at large heliocentric distances. Earth, Moon Planets 35, 203–212. http://dx.doi.org/10.1007/BF00058065.

Fraser, G.W., 2002. The ion detection efficiency of microchannel plates (MCPs). Int. J. Mass Spectrom. 215, 13–30. http://dx.doi.org/10.1016/S1387-3806(01)00553-X.

Freeman, J.W., Ibrahim, M., 1975. Lunar electric fields, surface potential and associated plasma sheaths. Moon 14, 103–114. http://dx.doi.org/10.1007/BF00562976.

Gazis, P.R., Lazarus, A.J., 1982. Voyager observations of solar wind proton temperature: 1-10AU. Geophys. Res. Lett. 9, 431–434. http://dx.doi.org/10.1029/GL009i004p00431.

Guernsey, R.L., Fu, J.H.M.F., 1970. Potential distribution surrounding a photo-emitting, plate in a dilute plasma. J. Geophys. Res. 75, 3193–3199.

Gulkis, S., Allen, M., Von Allmen, P., Beaudin, G., Biver, N., Bockelée-morvan, D., Choukroun, M., Crovisier, J., Davidsson, B.J.R., Encrenaz, P., Encrenaz, T., Frerking, M., Hartogh, P., Hofstadter, M., Ip, W., Janssen, M., Jarchow, C., Keihm, S., Lee, S., Lellouch, E., Leyrat, C., Rezac, L., Schloerb, F.P., Spilker, T., 2015. Subsurface properties and early activity of comet 67P/Churyumov-Gerasimenko. Science 347, 1–6 (80-.).

Gurevich, A.V., Pitaevskii, L.P., Smirnova, V.V., 1969. Ionospheric aerodynamics. Space Sci. Rev. 9, 805–871. http://dx.doi.org/10.1007/BF00226263.

Halekas, J.S., Poppe, A.R., McFadden, J.P., 2014. The effects of solar wind velocity distributions on the refilling of the lunar wake: ARTEMIS observations and comparisons to one-dimensional theory. J. Geophys. Res. Space Phys. 119, 5133–5149. http://dx.doi.org/10.1002/2014JA020083.

Halekas, J.S., Bale, S.D., Mitchell, L.D., Lin, R.P., 2005. Electrons and magnetic fields in the lunar plasma wake. J. Geophys. Res. 110, A07222. http://dx.doi.org/10.1029/2004JA010991.

Halekas, J.S., Saito, Y., Delory, G.T., Farrell, W.M., 2011. New views of the lunar plasma environment. Planet. Space Sci. 59, 1681–1694. http://dx.doi.org/10.1016/j.pss.2010.08.011.

Halekas, J.S., Delory, G.T., Lin, R.P., Stubbs, T.J., Farrell, W.M., 2008. Lunar Prospector observations of the electrostatic potential of the lunar surface and its response to incident currents. J. Geophys. Res. 113, A09102. http://dx.doi.org/10.1029/2008JA013194.

Halekas, J.S., Delory, G.T., Lin, R.P., Stubbs, T.J., Farrell, W.M., 2009. Lunar prospector measurements of secondary electron emission from lunar regolith. Planet. Space Sci. 57, 78–82. http://dx.doi.org/10.1016/j.pss.2008.11.009.

Halekas, J.S., Mitchell, D.L., Lin, R.P., Hood, L.L., Acuña, M.H., Binder, A.B., 2002. Evidence for negative charging of the lunar surface in shadow. Geophys. Res. Lett. 29, 771–774. http://dx.doi.org/10.1029/2001GL014428.

Hansen, K.C., Bagdonat, T., Motschmann, U., Alexander, C., Combi, M.R., Cravens, T. E., Gombosi, T.I., Jia, Y.-D., Robertson, I.P., 2007. The plasma environment of comet 67P/Churyumov-Gerasimenko throughout the Rosetta main mission. Space Sci. Rev. 128, 133–166. http://dx.doi.org/10.1007/s11214-006-9142-6.

Heggy, E., Palmer, E.M., Kofman, W., Clifford, S.M., Righter, K., Hérique, A., 2012. Radar properties of comets: Parametric dielectric modeling of Comet 67P/Churyumov–Gerasimenko. Icarus 221, 925–939. http://dx.doi.org/10.1016/j.icarus.2012.09.023.

Hill, T.W., Thomsen, M.F., Tokar, R.L., Coates, A.J., Lewis, G.R., Young, D.T., Crary, F.J., Baragiola, R.A., Johnson, R.E., Dong, Y., Wilson, R.J., Jones, G.H., Wahlund, J.E., Mitchell, D.G., Hornyi, M., 2012. Charged nanograins in the Enceladus plume. J. Geophys. Res. Space Phys. 117, 1–11. http://dx.doi.org/10.1029/2011JA017218.

Horányi, M., 1996. Charged dust dynamics in the solar system. Annu. Rev. Astron. Astrophys. 34, 383–418. http://dx.doi.org/10.1146/annurev.astro.34.1.383.

Huddleston, D.E., Johnstone, A.D., Coates, A.J., 1990. Determination of comet Halley gas emission characteristics from mass loading of the solar wind. J. Geophys. Res. 95, 21. http://dx.doi.org/10.1029/JA095iA01p00021.

Ip, W.-H., Axford, W.I., 1987. The formation of a magnetic-field-free cavity at comet Halley. Nature 325, 418–419. http://dx.doi.org/10.1038/325418a0.

Jones, G., 2012. Nanodust measurements by the Cassini Plasma Spectrometer. In: Mann, I., Meyer-Vernet, N., Czechowski, A. (Eds.), Nanodust in the Solar System: Discoveries and Interpretations. Springer Berlin Heidelberg, Berlin Heidelberg, pp. 119–132. http://dx.doi.org/10.1007/978-3-642-27543-2_6.

Jones, G.H., Roussos, E., Coates, A.J., Crary, F., 2011. Surface Charging of Saturn's moon Rhea. In: EPSC-DPS Joint Meeting. Nantes, p. 1467.

Jones, G.H., Arridge, C.S., Coates, A.J., Lewis, G.R., Kanani, S., Wellbrock, A, Young, D. T., Crary, F.J., Tokar, R.L., Wilson, R.J., Hill, T.W., Johnson, R.E., Mitchell, D.G., Schmidt, J., Kempf, S., Beckmann, U., Russell, C.T., Jia, Y.D., Dougherty, M.K., Waite, J.H., Magee, B. a, 2009. Fine jet structure of electrically charged grains in Enceladus' plume. Geophys. Res. Lett., 36; , pp. 1–6. http://dx.doi.org/10.1029/2009GL038284.

Juhász, A., Szegő, K., 1998. Charged dust dynamics above the surface of a comet far from the Sun. J. Geophys. Res. 103, 12015. http://dx.doi.org/10.1029/97JA02991.

Jurac, S., Baragiola, R.A., Johnson, R.E., Sittler, E.C., 1995. Charging of ice grains by low-energy plasmas: application to Saturn's E ring. J. Geophys. Res. 100, 14821. http://dx.doi.org/10.1029/95JA00521.

Kallio, E., Jarvinen, R., Dyadechkin, S., Wurz, P., Barabash, S., Alvarez, F., Fernandes, V.A., Futaana, Y., Harri, A.-M., Heilimo, J., Lue, C., Mäkelä, J., Porjo, N., Schmidt, W., Siili, T., 2012. Kinetic simulations of finite gyroradius effects in the lunar plasma environment on global, meso, and microscales. Planet. Space Sci. 74, 146–155. http://dx.doi.org/10.1016/j.pss.2012.09.012.

Katz, I., Parks, D.E., Mandell, M.J., Harvey, J.M., Brownell, D.H., Wang, S.S., Rotenberg, M., 1977. A Three Dimensional Dynamic Study of Electrostatic Charging in Materials.

Kempf, S., Beckmann, U., Srama, R., Horanyi, M., Auer, S., Grün, E., 2006. The electrostatic potential of E ring particles. Planet. Space Sci. 54, 999–1006. http://dx.doi.org/10.1016/j.pss.2006.05.012.

Kissel, J., Altwegg, K., Clark, B.C., Colangeli, L., Cottin, H., Czempiel, S., Eibl, J., Engrand, C., Fehringer, H.M., Feuerbacher, B., Fomenkova, M., Glasmachers, A., Greenberg, J.M., Grün, E., Haerendel, G., Henkel, H., Hilchenbach, M., von Hoerner, H., Höfner, H., Hornung, K., Jessberger, E.K., Koch, A., Krüger, H., Langevin, Y., Parigger, P., Raulin, F., Rüdenauer, F., Rynö, J., Schmid, E.R., Schulz, R., Silén, J., Steiger, W., Stephan, T., Thirkell, L., Thomas, R., Torkar, K., Utterback, N.G., Varmuza, K., Wanczek, K.P., Werther, W., Zscheeg, H., 2007. Cosima – high resolution time-of-flight secondary ion mass spectrometer for the analysis of cometary dust particles onboard Rosetta. Space Sci. Rev. 128, 823–867. http://dx.doi.org/10.1007/s11214-006-9083-0.

Koenders, C., Glassmeier, K.-H., Richter, I., Motschmann, U., Rubin, M., 2013. Revisiting cometary bow shock positions. Planet. Space Sci. 87, 85–95. http://dx.doi.org/10.1016/j.pss.2013.08.009.

Lee, P., 1996. Dust levitation on asteroids. Icarus 124, 181–194. http://dx.doi.org/10.1006/icar.1996.0197.

Maksimovic, M., Pierrard, V., Lemaire, J.F., 1997a. A kinetic model of the solar wind with Kappa distribution functions in the corona. Astron. Astrophys. 324, 725–734.

Maksimovic, M., Pierrard, V., Riley, P., 1997b. Ulysses electron distributions fitted with Kappa functions. Geophys. Res. Lett. 24, 1151–1154. http://dx.doi.org/10.1029/97GL00992.

Manka, R.H., 1973. Plasma and Potential at the Lunar Surface, in: Grard, R.J.L. (Ed.), Photon and Particle Interactions with Surfaces in Space: Proceedings of the 6th

ESLAB Symposium. Springer Netherlands, pp. 26–29. doi:10.1007/978-94-010-2647-5_22.
McComas, D.J., Barraclough, B.L., Funsten, H.O., Gosling, J.T., Santiago-Muñoz, E., Skoug, R.M., Goldstein, B.E., Neugebauer, M., Riley, P., Balogh, A., 2000. Solar wind observations over Ulysses' first full polar orbit. J. Geophys. Res. 105, 10419. http://dx.doi.org/10.1029/1999JA000383.
Mendis, D., Horányi, M., 2013. Dusty plasma effects in comets: expectations for Rosetta. Rev. Geophys. 51, 53–75. http://dx.doi.org/10.1002/rog.20005.
Mendis, D.A., Hill, J.R., Houpis, H.L.F., Whipple, E.C., 1981. On the electrostatic charging of the cometary nucleus. Astrophys. J. 249, 787. http://dx.doi.org/10.1086/159337.
Nitter, T., Havnes, O., Melandsø, F., 1998. Levitation and dynamics of charged dust in the photoelectron sheath above surfaces in space. J. Geophys. Res. 103, 6605. http://dx.doi.org/10.1029/97JA03523.
Nordheim, T.A., Jones, G.H., Roussos, E., Leisner, J.S., Coates, A.J., Kurth, W.S., Khurana, K.K., Krupp, N., Dougherty, M.K., Waite, J.H., 2014. Detection of a strongly negative surface potential at Saturn's moon Hyperion. Geophys. Res. Lett. 41, 7011–7018. http://dx.doi.org/10.1002/2014GL061127.
Phillips, J.L., Bame, S.J., Gary, S.P., Gosling, J.T., Scime, E.E., Forsyth, R.J., 1995. Radial and meridional trends in solar wind thermal electron temperature and anisotropy: ulysses. Space Sci. Rev. 72, 109–112. http://dx.doi.org/10.1007/BF00768763.
Poppe, A., Horányi, M., 2010. Simulations of the photoelectron sheath and dust levitation on the lunar surface. J. Geophys. Res. 115, A08106. http://dx.doi.org/10.1029/2010JA015286.
Poppe, A.R., Piquette, M., Likhanskii, A., Horányi, M., 2012a. The effect of surface topography on the lunar photoelectron sheath and electrostatic dust transport. Icarus 221, 135–146. http://dx.doi.org/10.1016/j.icarus.2012.07.018.
Poppe, A.R., Halekas, J.S., Delory, G.T., Farrell, W.M., Angelopoulos, V., McFadden, J.P., Bonnell, J.W., Ergun, R.E., 2012b. A comparison of ARTEMIS observations and particle-in-cell modeling of the lunar photoelectron sheath in the terrestrial magnetotail. Geophys. Res. Lett. 39, L01102. http://dx.doi.org/10.1029/2011GL050321.
Prialnik, D., Bar-nun, A., 1988. The formation of a permanent dust mantle and its effect on cometary activity. Icarus 74, 272–283. http://dx.doi.org/10.1016/0019-1035(88)90042-5.
Rosenberg, E.D., Prialnik, D., 2009. Fully 3-dimensional calculations of dust mantle formation for a model of Comet 67P/Churyumov–Gerasimenko. Icarus 201, 740–749. http://dx.doi.org/10.1016/j.icarus.2009.01.028.
Roussos, E., Krupp, N., Krüger, H., Jones, G.H., 2010. Surface charging of Saturn's plasma-absorbing moons. J. Geophys. Res. 115, A08225. http://dx.doi.org/10.1029/2010JA015525.
Rubin, M., Koenders, C., Altwegg, K., Combi, M.R., Glassmeier, K.-H., Gombosi, T.I., Hansen, K.C., Motschmann, U., Richter, I., Tenishev, V.M., Tóth, G., 2014. Plasma environment of a weak comet – predictions for comet 67P/Churyumov–Gerasimenko from multifluid-MHD and hybrid models. Icarus 242, 38–49. http://dx.doi.org/10.1016/j.icarus.2014.07.021.
Sagdeev, R.Z., Evlanov, E.N., Fomenkova, M.N., Prilutskii, O.F., Zubkov, B.V., 1989. Small-size dust particles near Halley's comet. Adv. Space Res. 9, 263–267. http://dx.doi.org/10.1016/0273-1177(89)90272-X.
Samir, U., Wright, K.H., Stone, N.H., 1983. The expansion of a plasma into a vacuum: basic phenomena and processes and applications to space plasma physics. Rev. Geophys. 21, 1631. http://dx.doi.org/10.1029/RG021i007p01631.
Santolík, O., Gurnett, D.A., Jones, G.H., Schippers, P., Crary, F.J., Leisner, J.S., Hospodarsky, G.B., Kurth, W.S., Russell, C.T., Dougherty, M.K., 2011. Intense plasma wave emissions associated with Saturn's moon Rhea. Geophys. Res. Lett. 38, L19204. http://dx.doi.org/10.1029/2011GL049219.
Sierks, H., Barbieri, C., Lamy, P.L., Rodrigo, R., Koschny, D., Rickman, H., Keller, H.U., Agarwal, J., A'Hearn, M.F., Angrilli, F., Auger, A.-T., Barucci, M.A., Bertaux, J.-L., Bertini, I., Besse, S., Bodewits, D., Capanna, C., Cremonese, G., Da Deppo, V., Davidsson, B., Debei, S., De Cecco, M., Ferri, F., Fornasier, S., Fulle, M., Gaskell, R., Giacomini, L., Groussin, O., Gutierrez-Marques, P., Gutierrez, P.J., Guttler, C., Hoekzema, N., Hviid, S.F., Ip, W.-H., Jorda, L., Knollenberg, J., Kovacs, G., Kramm, J.R., Kuhrt, E., Kuppers, M., La Forgia, F., Lara, L.M., Lazzarin, M., Leyrat, C., Lopez Moreno, J.J., Magrin, S., Marchi, S., Marzari, F., Massironi, M., Michalik, H., Moissl, L., Mottola, S., Naletto, G., Oklay, N., Pajola, M., Pertile, M., Preusker, F., Sabau, L., Scholten, F., Snodgrass, C., Thomas, N., Tubiana, C., Vincent, J.-B., Wenzel, K.-P., Zaccariotto, M., Patzold, M., 2015. On the nucleus structure and activity of comet 67P/Churyumov–Gerasimenko. Science 347, 1–5. http://dx.doi.org/10.1126/science.aaa1044 (80-.).
Singer, S.F., Walker, E.H., 1962. Electrostatic dust transport on the lunar surface. Icarus 1, 112–120. http://dx.doi.org/10.1016/0019-1035(62)90011-8.
Snodgrass, C., Tubiana, C., Bramich, D.M., Meech, K., Boehnhardt, H., Barrera, L., 2013. Beginning of activity in 67P/Churyumov–Gerasimenko and predictions for 2014–2015. Astron. Astrophys. 557, A33. http://dx.doi.org/10.1051/0004-6361/201322020.
Sternovsky, Z., Chamberlin, P., Horanyi, M., Robertson, S., Wang, X., 2008. Variability of the lunar photoelectron sheath and dust mobility due to solar activity. J. Geophys. Res. 113, A10104. http://dx.doi.org/10.1029/2008JA013487.
Stubbs, T.J., Farrell, W.M., Halekas, J.S., Burchill, J.K., Collier, M.R., Zimmerman, M.I., Vondrak, R.R., Delory, G.T., Pfaff, R.F., 2014. Dependence of lunar surface charging on solar wind plasma conditions and solar irradiation. Planet. Space Sci. 90, 10–27. http://dx.doi.org/10.1016/j.pss.2013.07.008.
Szego, K., Juhasz, A., Bebesi, Z., 2014. Possible observation of charged nanodust from comet 67P/Churyumov–Gerasimenko: an analysis for the ROSETTA mission. Planet. Space Sci. 99, 48–54. http://dx.doi.org/10.1016/j.pss.2014.05.007.
Tenishev, V., Combi, M., Davidsson, B., 2008. A global kinetic model for cometary comae: the evolution of the coma of the Rosetta target comet Churyumov–Gerasimenko throughout the mission. Astrophys. J., 659–677.
Tenishev, V., Combi, M.R., Rubin, M., 2011. Numerical simulation of dust in a cometary Coma: application to comet 67P/Churyumov-Gerasimenko. Astrophys. J. 732, 104. http://dx.doi.org/10.1088/0004-637X/732/2/104.
Thomas, N., Sierks, H., Barbieri, C., Lamy, P.L., Rodrigo, R., Rickman, H., Koschny, D., Keller, H.U., Agarwal, J., Hearn, M.F.A., Angrilli, F., Auger, A., Barucci, M.A., Kramm, J., Kührt, E., Küppers, M., Forgia, F. La, 2015. The morphological diversity of comet 67P/Churyumov-Gerasimenko. Science, 347; , pp. 1–7.
Tiersch, H., Notni, P., 1989. The electric potential on dust particles in comets and in interplanetary space. Astron. Nachr. (A J. all Fields Astron) 310, 67–78. http://dx.doi.org/10.1002/asna.2113100116.
Trotignon, J.G., Michau, J.L., Lagoutte, D., Chabassière, M., Chalumeau, G., Colin, F., Décréau, P.M.E., Geiswiller, J., Gille, P., Grard, R., Hachemi, T., Hamelin, M., Eriksson, A., Laakso, H., Lebreton, J.P., Mazelle, C., Randriamboarison, O., Schmidt, W., Smit, a, Telljohann, U., Zamora, P., 2006. RPC-MIP: the mutual impedance probe of the Rosetta plasma consortium. Space Sci. Rev., 128; , pp. 713–728. http://dx.doi.org/10.1007/s11214-006-9005-1.
Utterback, N.G., Kissel, J., 1990. Attogram dust cloud a million kilometers from Comet Halley. Astron. J. 100, 1315–1322. http://dx.doi.org/10.1086/115599.
Vigren, E., Galand, M., Lavvas, P., Eriksson, A.I., Wahlund, J.-E., 2015. On the possibility of significant electron depletion due to nanograin charging in the Coma of Comet 67P/Churyumov-Gerasimenko near perihelion. Astrophys. J. 798, 130. http://dx.doi.org/10.1088/0004-637X/798/2/130.
Weaver, H.A., Mumma, M.J., Larson, H.P., Davis, D.S., 1986. Post-perihelion observations of water in comet Halley. Nature 324, 441–444. http://dx.doi.org/10.1038/324441a0.
Wellbrock, A., Coates, A.J., Jones, G.H., Lewis, G.R., Waite, J.H., 2013. Cassini CAPS-ELS observations of negative ions in Titan's ionosphere: trends of density with altitude. Geophys. Res. Lett. 40, 4481–4485. http://dx.doi.org/10.1002/grl.50751.
Whipple, E.C., 1981. Potentials of surfaces in space. Rep. Prog. Phys. 44, 1197–1250. http://dx.doi.org/10.1088/0034-4885/44/11/002.
Zimmerman, M.I., Farrell, W.M., Poppe, A.R., 2014. Grid-free 2D plasma simulations of the complex interaction between the solar wind and small, near-earth asteroids. Icarus 238, 77–85. http://dx.doi.org/10.1016/j.icarus.2014.02.029.
Zouganelis, I., 2008. Measuring suprathermal electron parameters in space plasmas: implementation of the quasi-thermal noise spectroscopy with kappa distributions using in situ Ulysses/URAP radio measurements in the solar wind. J. Geophys. Res. 113, A08111. http://dx.doi.org/10.1029/2007JA012979.